Efficient perovskite solar cells by combination use of Au nanoparticles and insulating metal oxide

Zhang, Chenxi; Luo, Qi; Shi, Jianhua; Yue, Liyang; Wang, Zengbo; Chen, Xiaohong; Huang, Sumei

Nanoscale

DOI:
10.1039/C6NR09972F

Published: 01/01/2017

Peer reviewed version

View Article Online
DOI: 10.1039/C6NR09972F

Efficient Perovskite Solar Cells by Combination use of Au Nanoparticles and Insulating Metal Oxide

Chenxi Zhang[1], Qi Luo[1], Jianhua Shi[2], Liyang Yue[3], Zengbo Wang[3], Xiaohong Chen[1], Sumei Huang[*,1]

[1]Engineering Research Center for Nanophotonics & Advanced Instrument, Ministry of Education, School of Physics and Materials Science, East China Normal University, North Zhongshan Rd. 3663, Shanghai 200062, P. R. China

[2]New Energy Technology Center, Shanghai Institute of Microsystem and Information Technology, 865 Chang Ning Road, Shanghai 200050, P. R. China

[3]School of Electronic Engineering, Bangor University, Bangor LL57 1UT, UK.

Abstract

Simultaneously high open circuit voltage and high short circuit current density is a big challenge for achieving high efficient perovskite solar cells due to the complex excitonic nature of hybrid organic – inorganic semiconductors. Herein, we developed a facile and effective method to process efficient plasmonic PSC devices. The solar cells were prepared by incorporating Au nanoparticles (NPs) into mesoporous TiO_2 films and depositing MgO passivation film on the Au NP modified mesoporous titania by wet spinning and pyrolysis of the magnesium salt. The obtained PSCs by combinational use of Au NPs and MgO demonstrated a high power conversion

*)Corresponding author, email: smhuang@phy.ecnu.edu.cn

View Article Online
DOI: 10.1039/C6NR09972F

efficiency of 16.1 % with both high open circuit voltage of 1.09 V and high short-circuit current density of 21.76 mA cm^{-2}. The device achieved 34.2 % improvement of the power conversion efficiency compared with the device based on pure TiO_2. Moreover, a significant improvement of the UV stability in the perovsikite solar cell is achieved by combinational use of Au NPs and insulating MgO. The fundamental optics and physics behind regulation of energy flow in perovskite solar cell and concept of using Au nanoparticles and MgO to improve the device performance has been explored. The results indicate that the combinational use of Au nanparticles and MgO passivation film is an effective way in designing high performance and stability organic – inorganic perovskite photovoltaic materials.

Keywords: Perovskite solar cells, Au nanoparticles, MgO passivation layer, plasmon enhancement, near-field

View Article Online
DOI: 10.1039/C6NR09972F

1. INTRODUCTION

Photovoltaics has the potential to be the prime candidates for future energy sources and make a large contribution to solving the problem of climate change. Specially, inorganic–organic hybrid perovskite solar cells (PSCs) have provided a lasting impression on the scientific community because of their rapid progress as high efficient and low cost technology. Starting from the first well-known PSCs exploited the device structure of dye-sensitized solar cells (DSSCs) by replacing dye molecules with perovskite crystals in 2009, in only seven years power conversion efficiencies (PCEs) above 22% have already been reported and certified.[1-4] The latest certified PCE value of 22.1 % is approaching to that of commercial monocrystalline silicon solar cells.[4] Even though such rapid and unprecedented progress for any photovoltaic (PV) material, for instance, silicon, GaAs, CIGS and CdTe, further improvements for PSCs are expected and required in order to completely surpass the other PV technologies and fully realize their potential as solar cells.

In the past seven years, various perovskite absorber materials have been developed, forming a large family of crystalline materials. The most commonly used for PV devices have an ABX_3 chemical composition containing an organic cation A, such as methylammonium (MA)[2] or formamidinium (FA) [5], a divalent metal B, such as Pb[2] or Sn,[6] and a halide X, such as Br or I. These perovskites are processed by a large number of techniques ranging from spin coating,[2] dip coating,[7] two-step interdiffusion,[8] chemical vapour deposition,[9] thermal evaporation,[10] solvent

View Article Online
DOI: 10.1039/C6NR09972F

engineering,[11, 12] to intramolecular exchange processing.[13] Much of the work in the field of Inorganic–organic hybrid photovoltaics to date has been focused on developing new materials, technological process innovations and device structures to maximize the light absorption, charge separation and collection and voltage output. While we have some basic understanding of the PSC devices as an optical system, there have been limited attempts to exploit the optical designs to manage the light in-coupling and propagation as means to enhance the overall device performance.

One possible method for optical management and achieving fundamental efficiency enhancements in PSC devices is to utilize localized surface plasmon resonance (LSPR) in metallic nanostructures. Surface plasmons (SPs) are electron oscillations excited by either photons or electrons at the metal–dielectric interfaces, associated with well-confined surface electromagnetic waves.[14, 15] With proper engineering of the metal structures, such confinement can lead to an enhanced electromagnetic field at the metal–dielectric interfaces, which could be utilized for improvement of PV device efficiencies, helping to approach or even surpass the Shockley−Queisser limit without any exotic operating principles.[15, 16] The use of metal NPs and arrangements of them have been explored for almost all types of solar cells, for example, dye-sensitized,[17, 18] organic,[19] silicon, [20, 21] and PSC solar cells.[22, 23] As reported by Lee et al., Au NPs were doped in the PEDOT:PSS layer of the P3HT:PCBM device to induce the plasmonic enhancement for the active layer. [19] The PCE for the device with a low concentration of Au NPs was improved from 3.04 % to

View Article Online
DOI: 10.1039/C6NR09972F

3.65%. Slight plasmonic enhancements in the device PV performance were reported in most of the previous studies. In recent studies, nevertheless, Snaith and co-workers demonstrated that the employment of metal oxide (SiO_2, TiO_2) coated metal (Au, Ag) NPs into mesoporous Al_2O_3 scaffolds induced significant photocurrent enhancements in methylammonium lead iodide based devices.[22, 23] However, these enhancements could not be attributed to increased solar light absorption in the spectral regime of the metal nanoparticle LSPRs. The origin of the enhancement observed in plasmonic PSCs remains unknown. The presence of metal NPs may favor radiative decay of excitons, photon recycling, nonradiative photocarrier generation, light trapping, and help to reduction of the perovskite film thickness and hence decrease of the amount of lead present in the device.[15, 22-26] On the other hand, incorporated metal nanoparticles can act as sites for electron recombination. These factors can competitively have an impact on the performance and the development of the PSC device. Although there have been a few experimental evidences for plasmonic PSCs, many fundamental physical mechanisms are not systematically understood.

In this work, we report a facile and effective method to process efficient plasmonic PSC devices. Our investigation is very different from the previous reports. Au nanoparticles were incorporated into mesoporous TiO_2 films, chiefly on their top surfaces. Then, MgO passivation films were prepared on the Au NP modified mesoporous titania by wet spinning and pyrolysis of the magnesium salt. Our results showed that combination use of Au NPs and MgO significantly enhanced both the

View Article Online
DOI: 10.1039/C6NR09972F

current density and the photovoltage of the perovskite solar cells. The energy conversion efficiency of the Au NPs and MgO modified perovskite solar cell increased from 12.0 % to 16.1%. The fundamental optics and physics behind the plasmonic perovskite solar cell based on Au nanoparticles and insulating MgO was studied.

2. EXPERIMENTAL

All materials were purchased from either Alfa Aesar or Sigma-Aldrich, unless otherwise stated. CH_3NH_3I (MAI) was synthesized according to a previous study [12].

Au nanoparticles were prepared according to the method published previously with slight modification.[18] A 381 µl portion of hydrogen tetrachloroaurate (III) ($HAuCl_4 \cdot 3H_2O$) aqueous solution (0.1 M) was added into 150 ml DI water and brought to a rolling boil with stirring, and then 2 ml of 2% (wt.%) trisodium citrate dehydrate solution was added. After continuous boiling for about 5 min, the reduction of gold chloride was almost completed. The solution was removed from the heat source and allowed to cool naturally and sit overnight. The obtained solution was used as a seed solution for the Au NPs' preparation. 40 µl $HAuCl_4 \cdot 3H_2O$ solution, 24.9 µl hydroquinone and the seed solution were mixed in 50 ml DI water at room temperature under vigorously stirring over 30 min to obtain colloidal gold solutions with particle size around 40 nm.

View Article Online
DOI: 10.1039/C6NR09972F

Fluorine–doped tin oxide (FTO) coated slides (Pilkington TEC 15) were patterned by etching with Zn powders and 2 M HCl. The etched slides were then cleaned with liquid detergent, acetone, ethyl alcohol and de-ionized water for 15 min, respectively, to remove the organic or inorganic residues, and finally dried in a vacuum oven. Isopropyl titanate (200 μl) and 5 ml of ethanol were mixed to prepare a clear precursor sol. The precursor sol was spin-coated onto the Zn/HCl-etched FTO substrate at 4500 rpm, followed by annealing at 500 °C to form a compact TiO_2 layer. About 0.4 μm-thick mesoporous TiO_2 (p-TiO_2) layer was deposited on the c-TiO_2 by spin-coating TiO_2 paste (Dyesol 18NR-T) diluted in anhydrous ethanol (1:3.5, weight ratio) at 2000 r.p.m for 50 s. The layers were then sintered at 500 ºC for 30 minutes in air. After cooling down to the room temperature (RT), the samples were treated using the $TiCl_4$ aqueous solution at 70°C for 30 min and dried at 500 °C for 30 min. After the mesoporous film sample was cooled down to RT, 80 μl of Au NPs solution (0.19 mg/ml) was first spin-coated onto the mesoporous film surface, and the samples were heated at 100 ºC for 30 minutes on a hotplate in air. Then, the MgO precursor solution of $Mg(CH_3COO)_2$ in deionized water was spin-coated on the Au NPs treated p-TiO_2 layer at 3000 r.p.m for 30s, and then heated at 400 °C for 1 h to form MgO overlayer. The used concentrations of the magnesium salt were 90 mM. The perovskite layer was grown by a spin-coating process using a γ-butyrolactone (GBL) and dimethylsulphoxide (DMSO) solution of PbI_2 and CH_3NH_3I.[11, 12] The perovskite precursor solution was prepared by mixing CH_3NH_3I (0.1975 g) powders and lead iodide PbI_2 (0.5785 g) in GBL (700 μl) and DMSO (300 μl) at 60 °C for 12 h. The

View Article Online
DOI: 10.1039/C6NR09972F

formed precursor solution was deposited onto MgO/ Au NPs /p-TiO_2/c-TiO_2/FTO sample by a successive two-step spin-coating process, at 2000 r.p.m. for 30 s and at 3500 r.p.m. for 50 s, respectively. Anhydrous chlorobenzene was dripped onto the center of the sample in the second spin-stage during the spin-coating process. The perovskite-precursor coated sample was heated and dried on a hot plate at 120 °C for 30 min. Notably, at the present concentrations of perovskite solution, a capping layer of solid-perovskite film was formed on top of the mesoporous titanium dioxide.[12] The hole-transport layer (HTL) was deposited by spin-coating a spiro-OMeTAD solution at 4,000 r.p.m. for 30 s. The spin-coating solution was prepared by dissolving 0.0723 g spiro-MeOTAD, 28.8 μl 4-tert-butylpyridine, 17.5 μl of a stock solution of 0.520 g ml^{-1} lithium bis(trifluoromethylsulphonyl)imide in acetonitrile and 29 μl of a stock solution of 0.300 g ml^{-1} tris(2-(1H-pyrazol-1-yl)-4-tert-butylpyridine)cobalt(III) bis(trifluoromethylsulphonyl)imide in acetonitrile in 1 ml chlorobenzene. Finally, 100 nm thick Ag film with an active area of 0.1cm^2 was evaporated on the Spiro-OMeTAD-coated film.[27] In order to investigate the possible degradation and enhancement mechanisms in PSC devices by incorporating Au NPs in the active layers, we designed and fabricated four types of PSC devices without Au nanoparticle or MgO modification, only with Au NP modification, only with MgO coating and with both Au NP and MgO coating. The four kinds of devices were named as S1, S2, S3 and S4, respectively.

The morphology of Au NP and MgO modified p-TiO_2 films was characterized by

View Article Online
DOI: 10.1039/C6NR09972F

a high-resolution field emission scanning electron microscope (FESEM, Hitachi S4800). Optical spectra of the perovskite films on the differently structured mesoporous TiO_2 were examined and characterized by means of ultraviolet–visible light (UV–vis) spectrometer (Hitachi, U-3010). Photoluminescence (PL) spectra were recorded at RT temperature using a HORIBA Jobin Yvon fluoromax-4 fluorescence spectrophotometer with an excitation wavelength of 507 nm. Electrochemical impedance spectroscopy (EIS) measurements of PSCs were recorded with a galvanostat (PG30.FRA2, Autolab, EcoChemie B. V Utrecht, Netherlands). Photocurrent density–voltage (*J* - *V*) measurements were performed using an AM 1.5 solar simulator equipped with a 1000 W Xenon lamp (Model No. 91192, Oriel, USA). The solar simulator was calibrated by using a standard Silicon cell (Newport, USA). The light intensity was 100 mW cm^{-2} on the surface of the test cell. *J-V* curves were measured using a computer-controlled digital source meter (Keithley 2440) with the reverse direction. During device photovoltaic performance characterization, a metal aperture mask with an opening of about 0.09 cm^2 was used. External quantum efficiency (EQE) measurements (74125, Oriel，USA) were also carried out for these cells.

3. RESULTS AND DISCUSSION

Fig. 1 (a) shows current density versus voltage (*J-V*) characteristics of the fabricated four types of PSC devices (S1-S4). The corresponding PV parameters including short circuit current density (J_{SC}), open circuit voltage (V_{OC}), PCE and fill

View Article Online
DOI: 10.1039/C6NR09972F

factor (FF) are summarized in Table 1. Fig. 1 (b) shows the FESEM image of the top surface morphology the formed p-TiO2 layer containing Au NPs. Fig. 1 (c) shows the FESEM image of the cross-sectional FESEM picture of glass/FTO/c-TiO_2/Au Np modified p-TiO_2. From both SEM images, the size of Au NPs (white spheres) is about 40 nm in diameter, most of Au nanoparticles are distributed on the top surface of the p-TiO_2, and the thickness of the porous TiO2 layer is about 400 nm. The absorbance of the prepared Au NPs in ethanol was shown in Fig. 1 (d). From the figure, the SPR absorbance peak was at 526 nm. Fig. 1 (e) displays an energy diagram of materials for PSC devices with Au NP and MgO modification.

From Table 1, the reference device (S1) without Au NP or MgO coatings exhibits a V_{OC} of 0.94 V, J_{SC} of 19.49 mA cm^{-2} and FF of 0.66, resulting in a total PCE of 12.0%. After incorporating bare Au NPs between mesoporous TiO_2 and semiconductor perovskite, the device (S2) became poorer and exhibited a PCE of 10.7 %. The pure addition of Au NPs significantly decreased both the short-circuit current density and the fill factor. The device (S3) with pure MgO modification displayed a PCE of 15.1 %. Compared with the TiO_2-only device (S1), the V_{OC} value of S3 considerably increased from 0.94 to 1.08 V. The best cell was obtained with both Au NP and MgO coatings. It showed a short-circuit current density of 21.76 mA/cm^2, open-circuit voltage of 1.09 V and fill factor of 0.68, yielding the highest efficiency (η) of 16.1 %. Compared with the TiO_2-only device (S1), the power conversion efficiency (PCE) enhancement for the device incorporating Au NPs and

View Article Online
DOI: 10.1039/C6NR09972F

MgO mainly comes from the greatly improved short-circuit photocurrent *J*sc (19.49 to 21.76 mA/cm^2) and the open-circuit voltage V_{OC} (0.94 to 1.09 V), whilst the fill factor is only slightly changed.

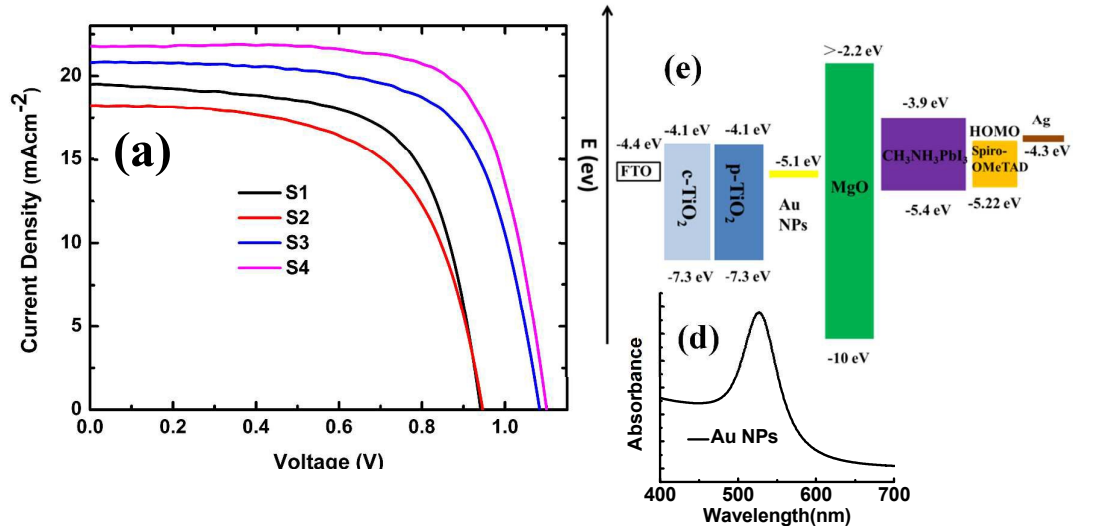

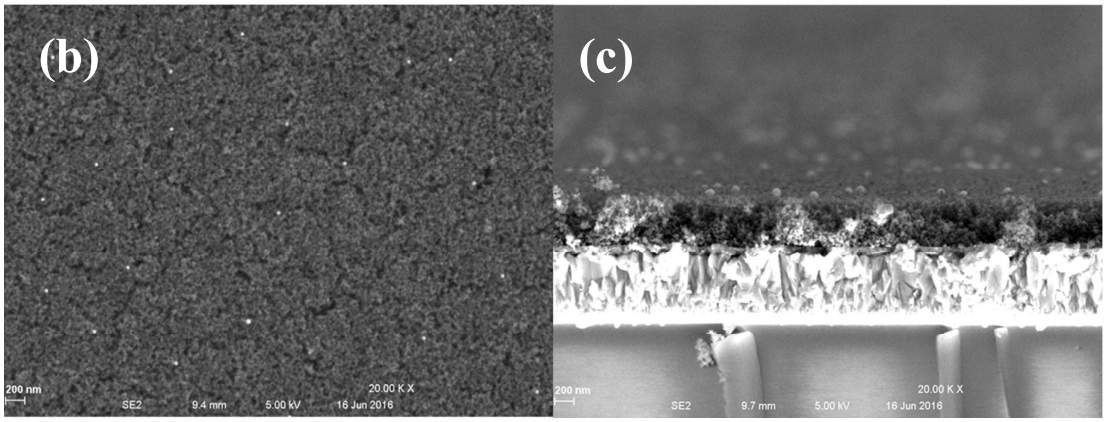

Fig. 1 (a) *J*-*V* curves of perovskite solar cells based on p-TiO$_2$ without and with Au NP and MgO coating. (b) FESEM image of the top surface morphology of the p-TiO$_2$ layer containing Au NPs and (c) cross-sectional FESEM picture of the p-TiO$_2$ containing Au NPs. (d) Absorbance spectrum of Au suspension. (e) Energy diagram of materials for PSC devices with Au NP and MgO modification.

View Article Online
DOI: 10.1039/C6NR09972F

Table 1 Parameters of PSCs based on mesoporous TiO_2 with and without Au NPs and MgO modification

Device	J_{SC}(mAcm^{-2})	V_{OC} (V)	FF	η (%)
S1	19.49	0.94	0.66	12.0
S2	18.21	0.95	0.62	10.7
S3	20.82	1.08	0.67	15.1
S4	21.76	1.09	0.68	16.1

From Table 1, purely incorporating Au NPs between mesoporous TiO_2 and perovskite greatly degraded the PV performance of the PSC device, especially its J_{SC} and FF values. The PV variance and degradation may be due to two reasons. First, the Au NPs can be etched by the halide during the processing $CH_3NH_3PbI_3$ absorber and the gold diffusion and migration into the perovskite material possibly take place in the thermal annealing treatment of the perovskite precursor films, causing detrimental and irreversible changes to the absorber. [27-29] Au migration into the perovskite material was found for PSC devices with metal contacts under thermal stress even at 70 °C.[28] This metal migration was observed to cause irreversible changes to the devices and in turn severely affected the device performance metrics. Second, the bare Au nanoparticles can act as charge recombination or trapping sites for light generated charge carriers due to the lower conduction energy level of the Au NPs than that of the TiO_2 as shown in Fig. 1 (e).[30, 31] Comparing with the reference device (S1), device S3 with pure MgO modification exhibited enhanced J_{SC}, FF and V_{OC} values. At the interface between TiO_2 NPs and perovskite materials, the injected photo-induced electrons may recombine with holes. This would deteriorate the J_{SC} and the V_{OC} in

View Article Online
DOI: 10.1039/C6NR09972F

PSC devices. The coating of n-type p-TiO_2 with ultrathin MgO dielectric shells is a general route to enhance the efficiency of solar cell devices. The introduced nanometer thick MgO interlayer acted as a "surface passivation layer" between the absorber and TiO_2 to obstruct the recombination between photo-induced electrons and holes across the interface. The improved photocurrent, photovoltage and fill factor for photovoltaic devices employing an ultrathin MgO layer has been well known in DSSCs.[32, 33] Recently, MgO was successfully used as a blocking layer between compact or mesoporous TiO_2 and perovskite layers to improve the cell performance.[34-37] The increase of the open-circuit voltage of device S3 compared to device S1 can be mainly attributed to the much higher conduction band of MgO than that of TiO_2, which would cause the conduction band of TiO_2 to shift towards MgO and result in a higher quasi-Fermi level under illumination and a higher *V*oc.[34,38] Additionally, the ultrathin layer of MgO could act as a tunneling barrier that retards the back recombination from TiO_2 to the hole transport material (HTM) in PSCs, thus, high *J*sc and FF were obtained.[34] Retarding of electron-hole recombination is also proved by electrochemical impedance spectroscopy (EIS). By incorporating both Au NPs and MgO in the PSC device, the PV performance was further improved. As a result, device S4 containing both Au NPs and MgO is superior to the other three types of PSC cells. The insulating MgO layer protected the Au NPs coated on the p-TiO_2 from corrosion or migration during the processing $CH_3NH_3PbI_3$ absorber. The MgO film also prevented the direct contact between Au and the perovskite semiconductor, or the hole conductor spiro-OMeTAD in device S4, inhibiting an unwanted charge

View Article Online
DOI: 10.1039/C6NR09972F

recombination pathway within the perovskite solar cell. MgO was found to change the surface state of TiO_2 and worked as an insulating layer to reduce charge recombination as reported in Refs. 34-37. In our work, MgO coating have more functions. In addition to the roles reported in Refs. 34-37, MgO coating acts as an insulating shell to protect Au NPs, make Au NPs intact and keep their structural and thermal stability during the following processing perovskite absorbers. Furthermore, compared with device S3 with pure MgO modification, device S4 exhibited similar V_{OC} and FF values, but significantly higher photocurrent. The increase of photocurrent in device S4 compared to device S3 suggested that localized surface plasmon resonance (LSPR) and electrical effects of Au NPs enhance the photovoltaic response of PSCs.[39, 40]

To investigate the effects of Au NPs and MgO in PSC in detail, we measured optical absorption spectra as well as photoluminescence spectra of samples. As the PSC devices have different structures which would influence the interface between the perovskite absorber and the porous TiO_2, it is expected to show different defect densities. The PL spectra were effective in exploring the recombination properties of light-excited electrons and holes in defected semiconductors. Fig. 2 shows the UV-Vis and the PL spectra of FTO/c-TiO_2/p-TiO_2/$CH_3NH_3PbI_3$ samples without or with Au or MgO modification. At a glance, it is clear that there is no significant change in the absorption spectra of the four kinds of absorber samples. This may be due to the extraordinarily high absorption coefficient of hybrid perovskite

View Article Online
DOI: 10.1039/C6NR09972F

$CH_3NH_3PbI_3$ and the small amount of Au metal NPs or MgO loaded on p-TiO_2. From Fig. 2 (b), all absorber samples show emission peaks at about 762 nm (excitation wavelength 507 nm), corresponding to an absorption onset at ~760 nm.[41] The peak position of the emission was almost consistent within the four samples, however, the PL intensity changed a lot. Compared to the case of the reference absorber without any modification, the PL intensity of the absorber incorporated with bare Au NPs exhibited an obvious increasing tendency, whilst the PL intensity displayed a more and more intensely decreasing tendency from the sample with pure MgO to the one with both Au and MgO modification. Notably, the perovskite absorber sample with bare Au NPs exhibited the highest PL signal, and the corresponding PSC device was expected to show a higher recombination rate of carriers than the cells based on the other samples. In contrast, a significantly stronger degree of PL quenching for both perovskite samples with MgO coating using the magnesium salt was observed, confirming that electron extraction from perovskite to TiO_2 NPs with MgO modification was more significant higher than to the pristine TiO_2. The perovskite sample with both Au NP and MgO modification showed the lowest peak intensity and the most intense degree of PL quenching, a strong indication for the rapidest charge transfer, the most effective electron extraction and the least charge accumulation, and thus prospectively the highest short-circuit current and the best PV performance.[42, 43] Therefore, the inclusion of Au NPs and MgO are unambiguously helpful for improvements in the ability for charge separation and collection, rapid charge transport, and enhanced photocurrent in the PSC device.

View Article Online
DOI: 10.1039/C6NR09972F

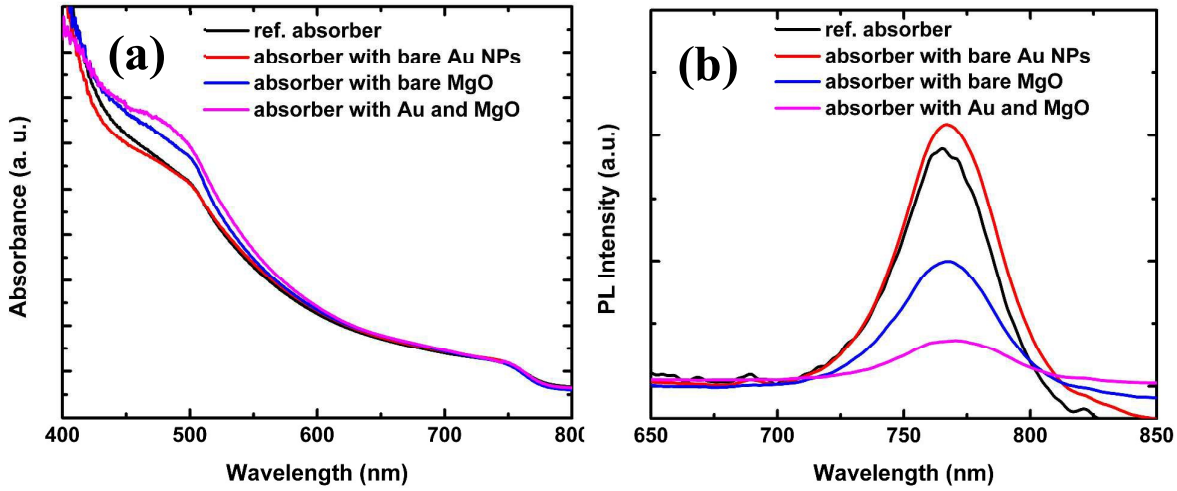

Fig. 2 (a) UV/Vis absorption and (b) PL spectra of p-TiO_2-based perovskite absorbers without and with Au NPs and MgO coating.

The retarding charge recombination behavior of the formed PSC cells was studied by measuring their dark *J-V* curves. Fig. 3 shows the measured dark *J-V* curves of the four structured PSC devices. As expected for device S3 and S4, MgO overlayer suppressed current almost at all biases, especially the dark cathodic recombination current at negative bias, compared to the case of the reference device (S1) without any modification. Device S2 with bare Au NPs showed the highest dark current value almost at all at all bias voltages, particularly at negative bias, because of the most intense charge carrier recombination. Recombination is one of the main factors limiting the cell performance. Device S4 with both Au NP and MgO modification showed the lowest dark current value at negative bias, demonstrating that combination use of Au NPs and MgO to modify porous TiO_2 in the $CH_3NH_3PbI_3$ absorbers is

View Article Online
DOI: 10.1039/C6NR09972F

crucial in preventing leakage. The incorporating both and Au NPs and MgO effectively and significantly blocked charge carrier recombination and thus promisingly enhanced the PV performance of perovskite solar cells. The bias voltage at the minimal current density for the device is possibly attributed to the accumulation of space charges at interface due to mobile ions in MgO@p-TiO_2 based perovskite solar cells.[27, 44]

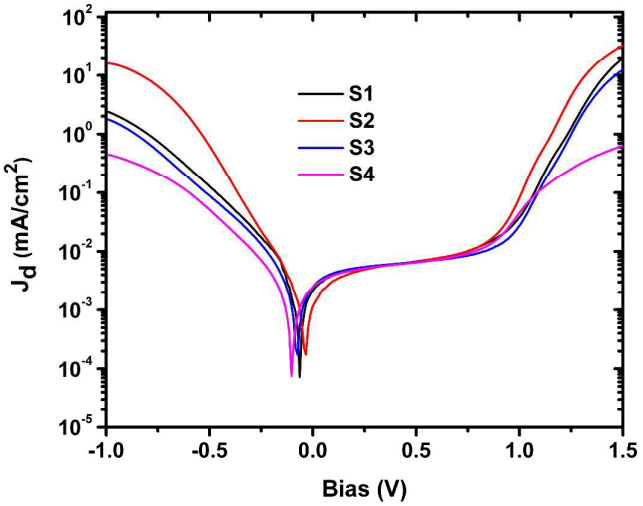

Fig. 3 Dark J-V curves of devices based on p-TiO_2 without and with Au NP and MgO coating.

Electrochemical impedance spectroscopy (EIS) was used to characterize internal resistance and charge transfer kinetics of p-TiO_2 based perovskite solar cells without and with Au NP or MgO modification. EIS measurements were performed for the four kinds of devices at a bias voltage of 0.9 V and in the dark. The measured Nyquist plot is shown in Fig. 4 (a). The structure of the PSC device could be considered as a leaking capacitor.[45] The semicircle visually represents the recombination resistance at

View Article Online
DOI: 10.1039/C6NR09972F

the interface of TiO_2/perovskite layer and TiO_2/hole transport layer. The bigger the diameter of the semicircle is, the less electron recombination at the interface. Moreover, the specific EIS results of PSCs can be estimated according to a simple equivalent circuit model shown in Fig. 4 (b), which has been widely applied for analyzing impedance spectroscopy of perovskite solar cells.[45] It is characterized by a recombination resistance, R_{rec}, in parallel with a chemical capacitance, $C_{rec,}$ and a hole transport resistance, R_{HTL}, in parallel with a chemical capacitance, C_{HTL}. The results of the impedance data are shown in Table 2. From Fig. 4(a) and Table 2, the device (S2) with bare Au NPs has the smallest semicircle, the minimal R_{rec} (83.9 $\Omega \cdot cm^2$), which indicates the lowest recombination resistance. The reference cell (S1) has the second lowest recombination resistance (116.0 $\Omega \cdot cm^2$). With pure MgO coated on the TiO_2 NP layer (S3), the diameter of the semicircle dramatically increases, which indicates overwhelmingly higher recombination resistance (375.0 $\Omega \cdot cm^2$) in the device with pure MgO modification than devices S1 and S2. The Rrec value (292.0 $\Omega \cdot cm^2$) of the PSC device containing both Au NPs and MgO is also much larger than the case of device S1 and S2, but a little smaller than that of device S3 with bare MgO. Our EIS measurement results indicate that the recombination resistance was increased 2.5-3.2 times after Au@MgO or pure MgO modification, which led to a significantly decrease in current loss through recombination and increased the photocurrent and enhanced the FF for both device S3 and S4 as shown in Table 1. Additionally, from Fig. 4 (a) and Table 2, the four structured PSC devices exhibit different series resistance, R_s, due to contact effects. Device S4 and S2 show the first and second

View Article Online
DOI: 10.1039/C6NR09972F

lowest series resistance Rs, respectively, indicating that addition of Au NPs can increase conductivity and improve the charge transport properties. Accordingly, the J_{SC} value of device S4 is higher than that of S3, and hence device S4 shows the highest efficiency.

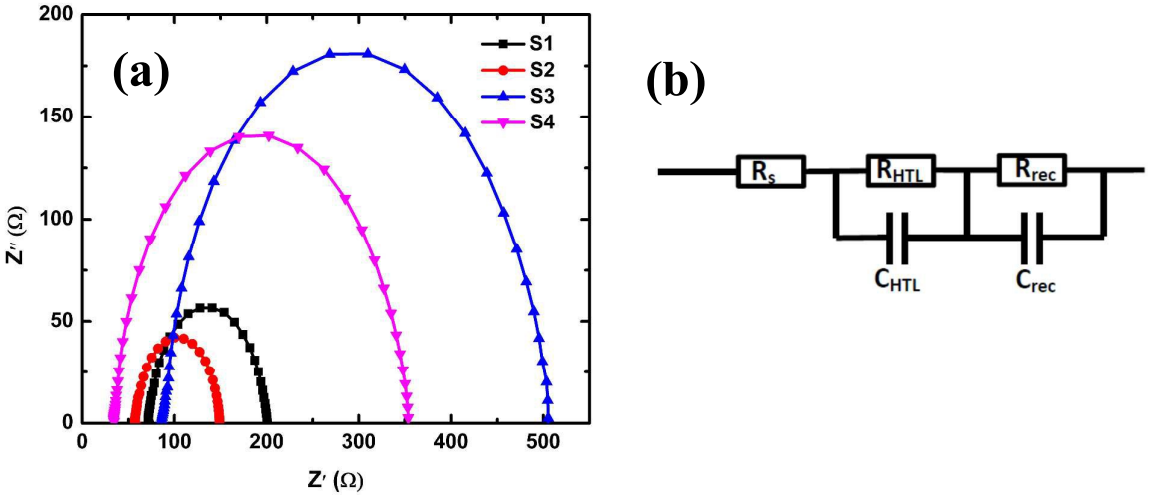

Fig. 4 (a) Nyquist plots of devices based on p-TiO_2 without and with Au NP and MgO coating under dark condition at 0.9 V applied bias. (b) Simplified equivalent circuit to fit the impedance spectra.

Table 2 EIS results of PSCs based on mesoporous TiO_2 with and without Au NPs and MgO modification.

Device	R_s ($\Omega \cdot cm^2$)	R_{rec} ($\Omega \cdot cm^2$)	C_{rec}($mF \cdot cm^{-2}$)	R_{HTL}($\Omega \cdot cm^2$)
S1	72.1	116.0	0.258	5.9
S2	57.0	83.9	0.255	2.9
S3	87.5	375.0	0.250	11.2
S4	34.5	292.0	0.254	5.4

View Article Online
DOI: 10.1039/C6NR09972F

EQE is more pertinent than photocurrent-voltage measurement for studying optical and electrical responses of PSCs. EQE can be a product of light-harvesting efficiency, electron injection efficiency from excited perovskite $CH_3NH_3PbI_3$ to TiO_2 nanoparticles, and electron collection efficiency at the cathode in a mesoscopic $CH_3NH_3PbI_3/TiO_2$ heterojunction solar cell. The corresponding EQE spectra of the fabricated four types of PSC devices (S1-S4) are shown in Fig.5 (a). EQE depends on the absorption of light, the electron injection efficiency and the collection of charges. In order to emphasize the positive contribution of Au NPs and MgO to the photocurrent, the EQE data of Au /or MgO modified PSCs were normalized by dividing that of the reference device, as shown in Fig. 5 (b). EQE of the PSC with pure MgO modification was significantly improved in the short wavelength region (320-600 nm) when compared with that of the pure TiO_2 based device. This result is corresponded well with the increase of the J_{SC} data given in Table 1. But the EQE enhancement of the pure MgO modified device basically decreased with the increase of the wavelength from 320 nm, and the EQE value at wavelength longer than about 750 nm was even lower than that of the reference cell. For an absorber semiconductor, the absorption coefficient, α, is related to the extinction coefficient, k, by $\alpha = 4\pi k/\lambda$, where λ is the wavelength. The absorption depth, l, is given by $l = \lambda/(p4\pi k)$, where p is the porosity, which is ~0.5 for the mesoporous $CH_3NH_3PbI_3$ layer and 1.0 for the perovskite capping layer. Light absorption depth of the absorber as a function of the light wavelength is shown in Fig. 5 (c). Photon capture is not as high in the range of $600 \text{ nm} < \lambda < 800 \text{ nm}$ as it is for shorter wavelengths because the extinction

View Article Online
DOI: 10.1039/C6NR09972F

coefficient rapidly decays for red frequencies. The thickness of the mesoporous layer in our devices is about 400 nm. The incident light at the longer wavelength (> 650 nm) is partially absorbed in the perovskite capping layer and the generated electron-hole pairs have to travel the greater distance to the surface of the networked TiO_2 NPs in the mesoporous layer, which makes it more difficult for electron injection into the insulator MgO coated TiO_2. As a result, the EQE spectrum of the device covered by MgO was lower than that of the reference in the long wavelength region (>750 nm). In contrast, EQE of the cell using bare Au NPs was considerably decreased in the short wavelength region (320-600 nm), as shown in Figs. 5 (a) and (b). However, the PSC containing both Au NPs and MgO achieved significant EQE enhancement across the whole UV-Vis- near infra-red (NIR) region (320- 800 nm) than the cell based on pure TiO_2. The EQE enhancement in the whole UV-Vis-NIR regime induced the prominent increase in J_{SC} for device S4. From Figs. 5 (a) and (b), the trend in EQE enhancement for differently structured PSC devices is also consisted with that from *J-V* measurement and analysis shown in Figure 1 and Table 1.

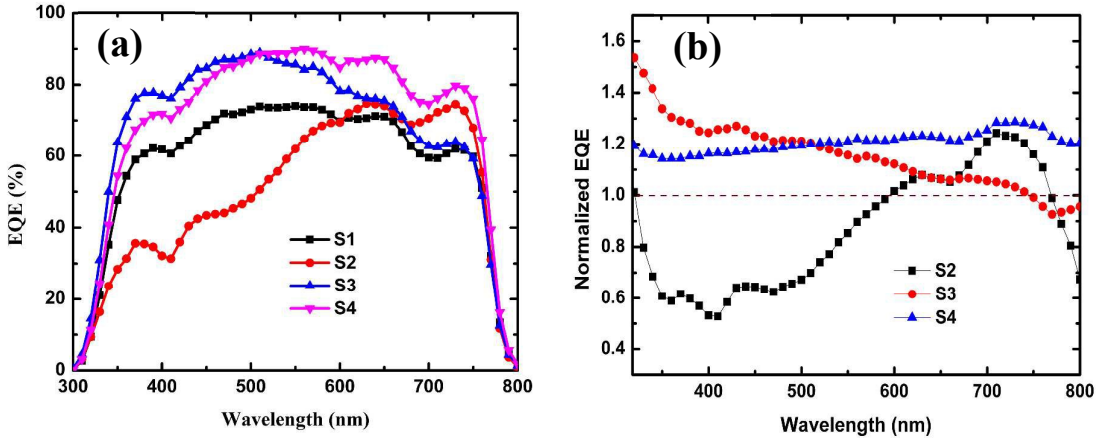

View Article Online
DOI: 10.1039/C6NR09972F

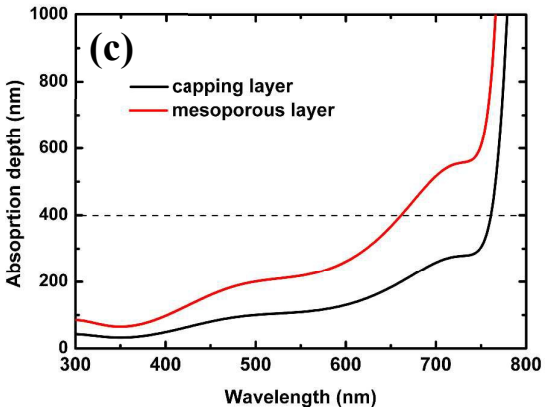

Fig.5 (a) EQE spectra and (b) normalized EQE curves of devices based on p-TiO_2 without and with Au NPs and MgO coating. (c) Calculated absorption depth as a function of wavelength.

As compared to bare Au NPs, Au NPs with insulating MgO shells have better structural and thermal stability, in particular retarding the corrosion of Au NPs by the halide, preventing charge trapping site formation or Oswald ripening[46] and enabling thermal processing of high-quality perovskite absorbers during the device fabrication. More importantly, from the standpoint of Au NPs, the insulating MgO coating prevents direct contact between Au and the perovskite, or the hole conductor spiro-OMeTAD, inhibiting an unwanted charge recombination pathway within the devices, while from the point of porous TiO_2, ultra-thin MgO coating on porous TiO_2 effectively blocks the charge recombination at the $TiO_2/CH_3NH_3PbI_3$ interface in perovskite solar cells, thereby extending the carrier lifetime and improving J_{SC} and V_{OC} values of the PSC device.[34, 35] As a result, employment of both Au NPs and MgO in the $CH_3NH_3PbI_3$ absorbers effectively and significantly enhanced J_{SC}, V_{OC} and

View Article Online
DOI: 10.1039/C6NR09972F

EQE values of perovskite solar cells.

Generally, metal nanoparticles could enhance the light energy capture in the solar cell by either scattering light enabling a longer optical path-length, by a dipole−dipole interaction and resonant energy transfer or by near-field coupling between the surface plasmon polariton and the absorber excited state. Two classic processes, i.e., light absorption increase by LSPRs[15-21, 26] and hot-electron injection,[25, 47- 49] have been widely reported for plasmon-enhanced solar energy harvesting. In the field of perovskite solar cells, Snaith and co-workers first reported plasmonic enhancement in perovskite solar cells in 2013.[22] They mixed core-shell Au@SiO_2 NPs into Al_2O_3 paste to prepare mesoporous Al_2O_3 scaffold, delivering a $CH_3NH_3PbI_{3-x}Cl_x$ device efficiency up to 11.4%. Compared to the control device, the photocurrent density of the device containing Au@SiO_2 NPs was improved by 14.5%. The authors have systemically carried out time-resolved and steady state photoluminescence (PL) measurements of the peroskite absorber with and without Au@SiO_2 NPs. The obtained enhancement in device performance was attributed to a three-fold reduction in exciton binding energy (EB) of the perovskite in the presence of Ag LSPR. Two years later, Snaith and co-workers blended core-shell Ag@TiO_2 NPs into Al_2O_3 paste to prepare mesoporous Al_2O_3 scaffold, boosting the $CH_3NH_3PbI_{3-x}Cl_x$ device efficiencies by 12.4 %.[23] Their photon-to-current conversion efficiency (IPCE) measurements revealed broad-band enhancement over the entire absorption spectrum, rather than in the spectral region of the Ag nanoparticle LSPR. Small changes in the

View Article Online
DOI: 10.1039/C6NR09972F

exciton EB cannot be expected to result in significant changes of photocurrent generation in the solar cell. The authors developed a theoretical model, which predicts that the presence of highly polarizable nanoparticles enhances the radiative decay of excitons and increases the reabsorption of emitted radiation, presenting a novel photon recycling scheme for enhancing the PSC performance. In another study,[25] Au nanoparticles were inserted into a compact TiOx layer, resulting in a 20 % increase in Spiro-OMeTAD HTM based planer heterojunction $CH_3NH_3PbI_{3-x}Cl_x$ solar cell. Improvements in J_{SC}, V_{OC} and FF were attributed to plasmon-mediated hot carrier injection from Au NPs to TiOx. In a recent study,[26] Au decorated TiO_2 nanofibers by an electro-spinning technique were applied to assemble mesoscopic $CH_3NH_3PbI_3$ perovskite solar cells. The PSC with pure TiO_2 nanofibers shows an efficiency of 11.16 %, while the device with Au decorated TiO_2 nanofibers achieves an efficiency of 14.92%. This improvement was attributed to the enhancement of light absorption by LSPR and reduced charge recombination in Au@TiO_2 nanofiber electrodes. Therefore, the type of metal nanostructures used (shape, size, composition, shell control) and their precise location with respect to the perovskite in solar cells as well as the kind of perovskites impact device performance enhancements. Moreover, the spontaneous polarization of perovskite crystals adds both complexity and potential for energy harvesting. Deeper understanding of the fundamental interactions between plasmonic nanostructures and perovskites is required for future optimization of both the light harvesting abilities and charge transport mechanisms in PSCs.

View Article Online
DOI: 10.1039/C6NR09972F

In our work, no significantly distinct difference was observed in absorption pattern of the fabricated four types of PSC devices, as shown in Fig. 2 (a), nevertheless, the EQE enhancement was achieved over the whole range, including the UV-Vis (320 nm to 500 nm) and NIR wavelength range (500 to 800 nm) for the device doped with Au and MgO, rather than following in the spectral region of the Au nanoparticle localized surface plasmon resonances shown in Fig. 1 (d). Therefore, the EQE and PV performance enhancements for Au@MgO devices could not directly be associated with the optical spectrum of the Au@MgO nanoparticles. To investigate the roles of Au NPs and MgO shell in the observed EQE and photocurrent, photovoltage and PCE improvements in the plasmonic PSC cells, finite-difference time-domain (FDTD) numerical simulations were performed for the geometry shown in Fig. 6 (a). The PSC is with a structure of glass (50)/FTO(100)/c-TiO_2(40)/p-TiO_2 + Au spheres + MgO + $MAPbI_3$ (300)/ spiro-MeOTAD(100)/Ag(30). The numbers in parentheses indicate the layer thicknesses in nanometers. The thickness of MgO is 2 nm. The size of TiO_2 spheres (yellow color) in the p-TiO_2 is 10 nm in diameter, the spacing between TiO_2@MgO spheres is 1 nm, and the gaps are filled by $MAPbI_3$. In order to see the TiO_2 spheres, the colors of both $MAPbI_3$ (light blue color) and MgO shell (light green color) is half transparent. There is a single Au@MgO sphere positioned at the top of p-TiO_2 @MgO and embedded in $MAPbI_3$ capping layer. The diameter of the Au sphere (red color) is 40 nm. The optical properties (refractive index, n and extinction coefficient, k) of materials are from the data in previous publications.[50,51] A commercial FIT software package (CST Microwave Studio 2006)

View Article Online
DOI: 10.1039/C6NR09972F

was used with Cartesian grids system (FDTD module).[21, 52, 53]

The boundary conditions along *x* and *y* axis is set to be 'periodic'. Upon choosing periodic boundary setting and a suitably refined computational grid (the maximum grid length was chosen as wavelength / 300 in the paper) in the simulation software, the corresponding numerical solution gives an accurate representation of the dynamics of the electromagnetic field. The Au sphere@MgO is placed along the z coordinate as shown in Fig. 6 (a). The origin of the coordinates is taken at the center of the Au sphere. The *xy* plane is set parallel to the surface of the glass substrate. Let the plane-wave electromagnetic field of wave vector *k* be incident from the bottom surface of the glass substrate. The wave propagates along the z coordinate, the electric vector is along the *x* coordinate, and the magnetic vector along the *y* coordinate.

Figs. 6 (b) and (c) show the calculated local amplitude enhancement distribution of the electric field $|E|$ in the *xz* plane at y=0 for an incident wave with a wavelength of 560 nm or 730 nm, respectively. The maximal EQE value was obtained at 560 nm, and the maximal EQE enhancement was achieved at 730 nm as shown in Figs. 5 (a) and (b). The circumferences of the Au@MgO and p-TiO_2@MgO spheres can be seen clearly from the calculated figures. The electric field is only slightly enhanced and localized around the Au sphere, and the maximum |E| enhancement factor is only about 1.5 at 560 nm. Differently, the electric field is significantly enhanced and

View Article Online
DOI: 10.1039/C6NR09972F

localized around the Au sphere, and the maximum |E| enhancement factor is up to 22.8 at 730 nm.

Figs. 6 (d)-(g) show the simulated power flow within the *xz* planes at y = 0, 10 nm for wavelengths of 560 nm and 730 nm, respectively. The positions of the Au@MgO and p-TiO2@MgO spheres can be observed clearly from the figures. For the incident visible light with a wavelength of 560 nm, the power flow successively passes through TiO_2@MgO NPs, the filled perovskite semiconductor, Au@MgO and perovskite capping layer with some deflections from the z coordinate around the surface of the Au sphere as shown in Figs. 6 (d) and (e). When the light with a wavelength of 730 nm is normally incident on the PSC device, the wave almost straight passes through TiO_2@MgO NPs and the filled perovskite semiconductor along the z coordinate. But, after the porous layer, the straight propagation of light power flow is replaced by complex whirls and circulates round the Au spheres and the perovskite in the capping layer as shown in Figs. 6 (f) and (g). The simulated power flow within the *xy* planes at *z* = 0, 18 nm is shown in Figs. 6 (h) and (k) for the wavelength of 730 nm. The relative positions of the p-TiO_2@MgO spheres can be seen in the background. The red circle indicates the position of the Au@MgO sphere. For the incident red light along the positive *z* coordinate, the Au@MgO sphere array manipulates the flow of the red energy and partially guides the red light into the *xy* plane of the absorber film in nanoscale and near-field regions，and as a result, some red energy flows parallel to the *xy* plane, more clearly shown in Fig. 6 (k). The light

View Article Online
DOI: 10.1039/C6NR09972F

energy passing through the absorber perovskite surrounding the Au sphere will be redirected toward the Au sphere, absorbed by the Au, and then, the light energy is transferred back to the perovskite material, as clearly shown in Figs. 6 (f) and (g). The Au NP absorbs lights via some portion of its surfaces, and then re-radiates energy into the absorber via other parts of the surfaces. Light power flows could circulate the near-field areas for multiple rounds due to interference of scattered and incident lights.[54]

The above calculation results indicate that the Au@MgO sphere array in the PSC device can modulate and deflect the energy flow direction in dipole–dipole coupling. This energy flow regulation can open a process which is different from the widely reported light absorption enhancement by LSPRs[15-21, 26] or hot-electron injection[25, 47-49] for plasmon-enhanced solar energy harvesting. In the this case, the plasmonic metal absorbs sunlight, converts the absorbed energy into localized surface plasmon resonance oscillations and transfers the plasmonic energy to the perovskite semiconductor via resonant energy transfer, which generates electron–hole pairs below and near the perovskite band edge[55, 56] and enhances the efficiency of the incident photon-to-electron conversion process for red frequencies in perovskite solar cells shown in Table 1 and Figs. 5 (a) and (b). Furthermore, we think that the photon management by use of Au NPs and MgO shell to minimize photonic and energy losses in the PSC device also offers promising scenarios for employing photon recycling to improve photoconversion efficiencies of perovskite solar cells.[23, 57-59] In

View Article Online
DOI: 10.1039/C6NR09972F

our plamonic PSC device, energy transport is not limited by diffusive carrier transport but can occur over long distances through multiple absorption-emission events. Photons are reabsorbed and re-emitted many times before an electron-hole pair is collected or a luminescent red photon escapes. Pazos-Outón et al. show that lead halide materials have luminescence properties similar to those of GaAs[57] and may, thus, also reach super high conversion efficiencies as GaAs semiconductor materials. The presence of Au NPs enhances the radiative decay of excitons in the perovskite absorber[23]. The Au@MgO nanoparticles could work as antennas for the excitonic dipoles. The radiated photons from exciton decay would then have a dramatically prolonged optical path length due to the energy flow regulatory benefit of the Au nanospheres shown in Figs. 6 (f)-(k). By this means the reabsorption from reemitted light is enhanced, in essence enabling photon recycling with a much greater efficiency and driving the enhanced EQE and photocurrent in perovskite solar cells with the addition of Au nanoparticles and MgO compared to the case modified only with pure MgO.[23, 57-59] Higher photon densities also lead to higher internal luminescence and a buildup of excited charges, which increase the split of quasi-Fermi levels and enhance the achievable open-circuit voltage in a solar cell.[57, 60] Finally, introducing Au NPs in TiO_2 photoanodes of PSCs can increase the charge transport capability as demonstrated in Fig. 4 (a) and Table 2. As a result, employment of both Au NPs and MgO in the $CH_3NH_3PbI_3$ absorbers effectively and significantly enhanced EQE, J_{SC} and hence PCE values of perovskite solar cells compared to the case modified only with pure MgO shown in Table 1.

View Article Online
DOI: 10.1039/C6NR09972F

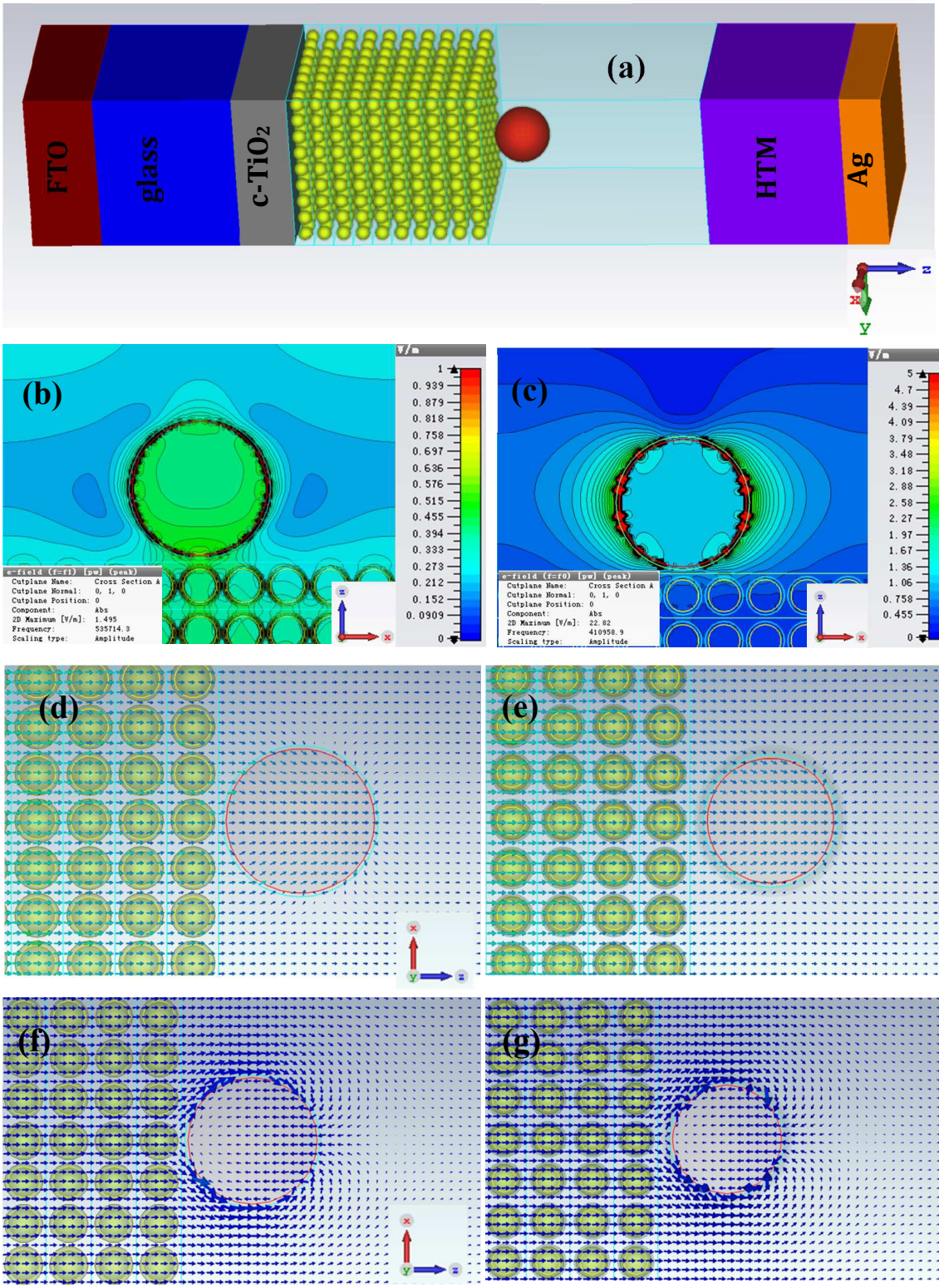

View Article Online
DOI: 10.1039/C6NR09972F

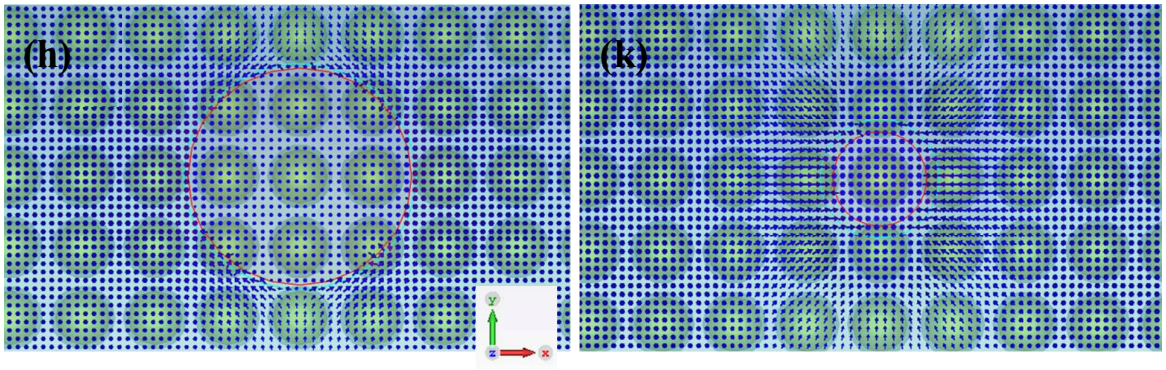

Fig.6 (a) Model of device modified with both Au NPs and MgO. 2D field $|E|$ enhancement distribution image in the xz planes at (b) y = 0 nm, λ=560 nm, (c) y= 0 nm, λ=730 nm. Power flow diagrams within the *xz* planes at (d) y = 0 nm, λ=560 nm, (e) y = 10 nm, λ=560 nm, (f) y= 0 nm, λ=730 nm, (g) y=10 nm, λ=730 nm. Power flow diagrams within the *xy* planes at (h) z= 0 nm, λ=730 nm, (g) z=18 nm, λ=730 nm.

The stability of perovskite solar cells is a major issue restricting the terrestrial applications. We investigated the stability of unsealed PSCs based on mesoporous TiO_2 with and without Au NPs and MgO modification under UV irradiation. The PSCs were exposed to 365 nm UV illumination with an intensity of 90 $mWcm^{-2}$, and removed at certain time intervals to measure the J-V curves under simulated AM1.5 100 $mWcm^{-2}$ irradiance. In Fig. 7 we observe that device S3 and S4 exhibit significantly improved stability. Their PCE remains more than 85%-90% of its initial value even after 15 min UV irradiation in air. By contrast, device S2 with bare Au NPs cannot endure the UV irradiation test and shows nearly zero PCE just after 1 min

View Article Online
DOI: 10.1039/C6NR09972F

UV irradiation, and the control device (S1) exhibits only 35% of its initial value after 9 min UV illumination under the same UV testing conditions. When TiO_2 based PSCs are exposed to UV light exposure, photo generated holes in the mesoporous TiO_2 react with oxygen absorbed at surface oxygen vacancies, which then become deep traps leading to charge recombination, resulting in a drop off in PV performance of the device.[61] Additionally, the UV light absorbed by TiO_2 would catalyze the decomposition of $CH_3NH_3PbI_3$ to PbI_2, forming non-radiative defect sites within the perovskite and especially at the TiO_2/perovskite interface and degrading the PV performance of the device.[62, 63] The presence of bare Au NPs in the PSC device dramatically accelerated the UV degradation, and the device with bare Au NPs deteriorated to zero efficiency in 2 min. These UV light effects can be avoided by depositing nanometer thick passivation layer onto the TiO_2 to prevent contact between TiO_2 and $CH_3NH_3PbI_3$, decrease the photocatalytic properties of the TiO_2 and reduce electronic defect density at the TiO_2/perovskite interface. It was reported that light stability of PSC devices was obviously improved by using CsBr as an interface modifier for the c-TiO_2[62] or employing Sb_2S_3 as the insulating layer between mesoporous TiO_2 and perovskite layers.[63] In our work, we have demonstrated that by incorporating both Au NPs and insulating MgO onto mesoporous TiO_2 a significant improvement of the UV stability in the perovsikite solar cell is achieved.

View Article Online
DOI: 10.1039/C6NR09972F

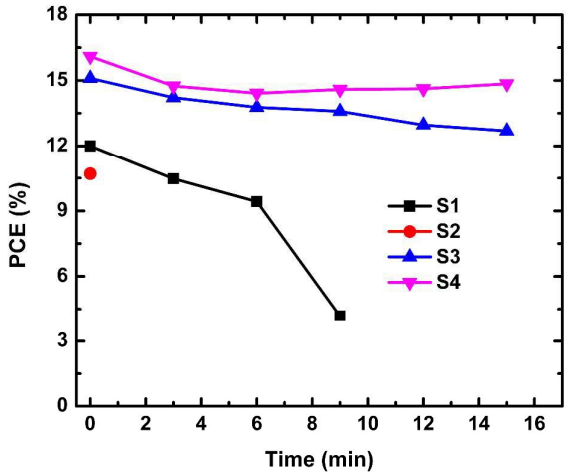

Fig. 7 Power conversion efficiency variation of unsealed PSCs based on mesoporous TiO_2 with and without Au NPs and MgO modification at ~55% humidity after various UV exposure durations (90 $mWcm^{-2}$ at 365 nm) durations.

4. CONCLUSIONS

A facile and effective method has been investigated to achieve efficient performance perovskite devices with simultaneously high open circuit voltage and high short circuit current density by combinational use of Au NPs and insulating MgO. Purely incorporating Au NPs between mesoporous TiO_2 and perovskite capping layer greatly degraded the PV performance of the PSC device from 12.0 % to 10.7 %. By employing a pure MgO nanolayer, the power conversion efficiency was increased from 12.0% to 15.1 %. By combinational use of Au NPs and MgO passivation layer, a high power conversion efficiency of 16.1 % with both high open circuit voltage of 1.09 V and high short-circuit current density of 21.76 mA cm^{-2} was obtained. The photovoltage, photocurrent and efficiency values were 16.0 %, 11.6 % and 34.2% higher than the pure TiO_2 based perovskite solar cells. The enhancement could be

View Article Online
DOI: 10.1039/C6NR09972F

associated with the effective photon management by use of Au NPs and MgO shell to minimize photonic and energy losses for the generation of carriers, the high charge transport capability and the low charge recombination losses in perovskite solar cells. Moreover, combinational use of Au NPs and MgO passivation layer effectively enhanced the stability of PSC devices under UV light soaking. The fundamental optics and physics behind regulation of energy flow in perovskite solar cell and concept of using Au nanoparticles and MgO to improve the device performance has been explored. Theoretical electromagnetic calculations supported the experimental plasmon-enhanced energy conversion efficiency results of perovskite solar cells in combination with Au NPs and MgO coating.

ACKNOWLEDGEMENTS

This work was supported by the National Natural Science Foundation of China (Nos. 11274119 and 61275038) and the Large Instruments Open Foundation of East China Normal University.

View Article Online
DOI: 10.1039/C6NR09972F

REFERENCES

1. A. Kojima, K. Teshima, Y. Shirai and T. Miyasaka, Organometal Halide Perovskites as Visible-Light Sensitizers for Photovoltaic Cells, *J. Am. Chem. Soc.*, 2009, **131**, 6050-6051.
2. M.M. Lee, J. Teuscher, T. Miyasaka, T.N. Murakami and H.J. Snaith, Supporting Material: Efficient hybrid solar cells based on meso-superstructured organometal halide perovskites, Science, 2012, **338,** 643.
3. N.J. Jeon, J.H. Noh, W.S. Yang, Y.C. Kim, S. Ryu, J. Seo and I.S. Sang, Compositional engineering of perovskite materials for high-performance solar cells, *Nature*, 2015, **517**, 476-480.
4. M.K. Nazeeruddin, In retrospect: Twenty-five years of low-cost solar cells, *Nature*, 2016, **538**, 463-464.
5. G.E. Eperon, S.D. Stranks, C. Menelaou, M.B. Johnston, L.M. Herz and H.J. Snaith, Formamidinium lead trihalide: a broadly tunable perovskite for efficient planar heterojunction solar cells, *Energ. Environ. Sci.*, 2014, **7**, 982-988.
6. N.K. Noel, S.D. Stranks, A. Abate, C. Wehrenfennig, S. Guarnera, A.-A. Haghighirad, A. Sadhanala, G.E. Eperon, S.K. Pathak and M.B. Johnston, Lead-free organic–inorganic tin halide perovskites for photovoltaic applications, *Energ. Environ. Sci.*, 2014, **7**, 3061-3068.
7. J. Burschka, N. Pellet, S.-J. Moon, R. Humphry-Baker, P. Gao, M.K. Nazeeruddin and M. Grätzel, Sequential deposition as a route to high-performance perovskite-sensitized solar cells, *Nature,* 2013, **499**, 316-319.
8. Z. Xiao, C. Bi, Y. Shao, Q. Dong, Q. Wang, Y. Yuan, C. Wang, Y. Gao and J. Huang, Efficient, high yield perovskite photovoltaic devices grown by interdiffusion of solution-processed precursor stacking layers, *Energ. Environ. Sci.*, 2014, **7**, 2619-2623.
9. Q. Chen, H. Zhou, Z. Hong, S. Luo, H.-S. Duan, H.-H. Wang, Y. Liu, G. Li and Y. Yang, Planar heterojunction perovskite solar cells via vapor-assisted solution process, *J. Am. Chem. Soc.*, 2013, **136**, 622-625.

View Article Online
DOI: 10.1039/C6NR09972F

10. M. Liu, M.B. Johnston and H.J. Snaith, Efficient planar heterojunction perovskite solar cells by vapour deposition, *Nature*, 2013, **501**, 395-398.
11. N.J. Jeon, J.H. Noh, Y.C. Kim, W.S. Yang, S. Ryu and S.I. Seok, Solvent engineering for high-performance inorganic–organic hybrid perovskite solar cells, Nat. Mater., 2014, **13**, 897-903.
12. C. Zhang, Y. Luo, X. Chen, Y. Chen, Z. Sun and S.M. Huang, Effective Improvement of the Photovoltaic Performance of Carbon-Based Perovskite Solar Cells by Additional Solvents, *Nano-Micro. Lett.*, 2016, **8**, 347-357.
13. M. Saliba, T. Matsui, J.-Y. Seo, K. Domanski, J.-P. Correa-Baena, M.K. Nazeeruddin, S.M. Zakeeruddin, W. Tress, A. Abate and A. Hagfeldt, Cesium-containing triple cation perovskite solar cells: improved stability, reproducibility and high efficiency, *Energ. Environ. Sci.*, 2016, **9**, 1989-1997.
14. S.M. Huang, M.H. Hong, B.S. Luk'Yanchuk and T.C. Chong, Direct and subdiffraction-limit laser nanofabrication in silicon, *Appl. Phys. Lett.*, 2003, **82**, 4809-4811.
15. H.A. Atwater and A. Polman, Plasmonics for improved photovoltaic devices, *Nat. Mater.*, 2010, **9**, 205-213.
16. W. Shockley and H.J. Queisser, Detailed balance limit of efficiency of p‐n junction solar cells, *J. Appl. Phys.*, 1961, **32**, 510-519.
17. B. Ding, B.J. Lee, M. Yang, H.S. Jung and J.K. Lee, Surface‐Plasmon Assisted Energy Conversion in Dye‐Sensitized Solar Cells, *Adv. Energy. Mater.*, 2011, **1**, 415-421.
18. D. Zhang, M. Wang, A.G. Brolo, J. Shen, X. Li and S.M. Huang, Enhanced performance of dye-sensitized solar cells using gold nanoparticles modified fluorine tin oxide electrodes, *J. Phys. D. Appl. Phys.*, 2012, **46**, 32-44.
19. H.L. Ji, J.H. Park, J.S. Kim, Y.L. Dong and K. Cho, High efficiency polymer solar cells with wet deposited plasmonic gold nanodots, *Org. Electron.*, 2009, **10**, 416-420.
20. D.M. Schaadt, B. Feng and E.T. Yu, Enhanced semiconductor optical absorption via surface plasmon excitation in metal nanoparticles, *Appl. Phys. Lett.*, 2005, **86**,

View Article Online
DOI: 10.1039/C6NR09972F

063106-063106-3.

21. Y. Chen, Z. Li, X. Chen, C. Liu, X. Ye, Z. Wang, Z. Sun and S. Huang, Improved performance of flexible amorphous silicon solar cells with silver nanowires, *J. Appl. Phys.*, 2012, **112**, 124320.
22. W. Zhang, M. Saliba, S.D. Stranks, Y. Sun, X. Shi, U. Wiesner and H.J. Snaith, Enhancement of perovskite-based solar cells employing core–shell metal nanoparticles, *Nano. Lett.*, 2013, **13**, 4505-4510.
23. M. Saliba, W. Zhang, V.M. Burlakov, S.D. Stranks, Y. Sun, J.M. Ball, M.B. Johnston, A. Goriely, U. Wiesner and H.J. Snaith, Plasmonic‐Induced Photon Recycling in Metal Halide Perovskite Solar Cells, *Adv. Funct. Mater.* , 2015, **25**, 5038-5046.
24. W.R. Erwin, H.F. Zarick, E.M. Talbert and R. Bardhan, Light trapping in mesoporous solar cells with plasmonic nanostructures, *Energ. Environ. Sci.*, 2016, **9**, 1577-1601.
25. Z. Yuan, Z. Wu, S. Bai, Z. Xia, W. Xu, T. Song, H. Wu, L. Xu, J. Si, Y. Jin and B. Sun, Hot‐Electron Injection in a Sandwiched TiO_x–Au–TiO_x Structure for High‐Performance Planar Perovskite Solar Cells, *Adv. Energy. Mater.*, 2015, **5**, 150038.
26. S.S. Mali, C.S. Shim, H. Kim, P.S. Patil and C.K. Hong, In situ processed gold nanoparticle-embedded TiO_2 nanofibers enabling plasmonic perovskite solar cells to exceed 14% conversion efficiency, *Nanoscale*, 2016, **8**, 2664-2677.
27. Z. Jiang, X. Chen, X. Lin, X. Jia, J. Wang, L. Pan, S.M. Huang, F. Zhu and Z. Sun, Amazing stable open-circuit voltage in perovskite solar cells using AgAl alloy electrode, *Sol. Energer. Mat. Sol. C*, 2016, **146**, 35-43.
28. K. Domanski, J.-P. Correa-Baena, N. Mine, M.K. Nazeeruddin, A. Abate, M. Saliba, W. Tress, A. Hagfeldt and M. Grätzel, Not All That Glitters is Gold: Metal Migration-Induced Degradation in Perovskite Solar Cells, *ACS nano*, 2016, **10,** 6306-6314.
29. Y. Luo, X. Chen, C. Zhang, J. Li, J. Shi, Z. Sun, Z. Wang, and S. Huang, AgAl alloy electrode for efficient perovskite solar cells, *RSC Adv.*, 2015, **5**,

View Article Online
DOI: 10.1039/C6NR09972F

56037-56044.

30. M. Gratzel, Photoelectrochemical cells, *Nature*, 1982, **414**, 338.
31. V. Subramanian, E.E. Wolf and P.V. Kamat, Catalysis with TiO_2/gold nanocomposites. Effect of metal particle size on the Fermi level equilibration, *J. Am. Chem. Soc.*, 2004, **126**, 4943-4950
32. H.S. Jung, J.-K. Lee, M. Nastasi, S.-W. Lee, J.-Y. Kim, J.-S. Park, K.S. Hong and H. Shin, Preparation of nanoporous MgO-coated TiO_2 nanoparticles and their application to the electrode of dye-sensitized solar cells, *Langmuir*, 2005, **21**, 10332-10335.
33. T. Taguchi, X.T. Zhang, I. Sutanto, K. Tokuhiro, T.N. Rao, H. Watanabe, T. Nakamori, M. Uragami and A. Fujishima, Improving the performance of solid-state dye-sensitized solar cell using MgO-coated TiO_2 nanoporous film, *Chem. Commun.*, 2003, **19**, 2480-2481.
34. J. Wang, M. Qin, H. Tao, W. Ke, Z. Chen, J. Wan, P. Qin, L. Xiong, H. Lei and H. Yu, Performance enhancement of perovskite solar cells with Mg-doped TiO_2 compact film as the hole-blocking layer, *Appl. Phys. Lett.,* 2015, **106**, 591.
35. X. Guo, H. Dong, W. Li, N. Li and L. Wang, Multifunctional MgO Layer in Perovskite Solar Cells, *ChemPhysChem*, 2015, **16**, 1727-1732.
36. Y. Yue, X. Yang, Y. Wu, N. T. Salim, A. Islam, T. Noda and L. Han, Selective Deposition of Insulating Metal Oxide in Perovskite Solar Cells with Enhanced Device Performance, *ChemSusChem*, 2015, **8**, 2625–2629.
37. L. Gouda, R. Gottesman, A. Ginsburg, D.A. Keller, E. Haltzi, J. Hu, S. Tirosh, A.Y. Anderson, A. Zaban and P.P. Boix, Open circuit potential build-up in perovskite solar cells from dark conditions to 1 sun, *J. Phys. Chem. Lett.*, 2015, **6**, 4640–4645.
38. H. J. Snaith and C. Ducati, SnO_2-Based Dye-Sensitized Hybrid Solar Cells Exhibiting Near Unity Absorbed Photon-to-Electron Conversion Efficiency, *Nano Lett.*, 2010, **10**, 1259–1265.
39. H.W. Dong, D.Y. Kim, K.W. Choi, J.H. Seo, S.H. Im, J.H. Park, O.O. Park and A.J. Heeger, Rücktitelbild: Enhancement of Donor–Acceptor Polymer Bulk

View Article Online
DOI: 10.1039/C6NR09972F

Heterojunction Solar Cell Power Conversion Efficiencies by Addition of Au Nanoparticles, *Angew.Chem.*, 2011, **50**, 5519-5523.

40. K. Catchpole and A. Polman, Plasmonic solar cells, *Opt. Express*., 2008, **16,** 21793-21800.
41. J.-H. Im, C.-R. Lee, J.-W. Lee, S.-W. Park and N.-G. Park, 6.5% efficient perovskite quantum-dot-sensitized solar cell, *Nanoscale*, 2011, **3**, 4088-4093.
42. G. Zhu, T. Lin, X. Lü, W. Zhao, C. Yang, Z. Wang, H. Yin, Z. Liu, F. Huang and J. Lin, Black brookite titania with high solar absorption and excellent photocatalytic performance, *J. Mater. Chem. A*, 2013, **1**, 9650-9653.
43. C. Huang, C. Liu, Y. Di, W. Li, F. Liu, L. Jiang, J. Li, X. Hao and H. Huang, Efficient Planar Perovskite Solar Cells with Reduced Hysteresis and Enhanced Open Circuit Voltage by Using PW12–TiO_2 as Electron Transport Layer, *ACS Appl. Mater. Inter.*, 2016, **8**, 8520-8526.
44. H. Zhang, C. Liang, Y. Zhao, M. Sun, H. Liu, J. Liang, D. Li, F. Zhang and Z. He, Dynamic interface charge governing the current–voltage hysteresis in perovskite solar cells, *Phys. Chem. Chem. Phys.*, 2015, **17**, 9613-9618.
45. P.P. Boix, G. Larramona, A. Jacob, B. Delatouche, I. Mora-Seróand J. Bisquert, Hole transport and recombination in all-solid Sb2S3-sensitized TiO_2 solar cells using CuSCN as hole transporter, *J. Phys. Chem. C*, 2011, **116**, 1579-1587.
46. M.D. Brown, T. Suteewong, R.S.S. Kumar, V. D'Innocenzo, A. Petrozza, M.M. Lee, U. Wiesner and H.J. Snaith, Plasmonic Dye-Sensitized Solar Cells Using Core−Shell Metal−Insulator Nanoparticles, *Nano. Lett.*, 2011, **11**, 438-445.
47. A. Furube, L. Du, K. Hara, R. Katoh and M. Tachiya, Ultrafast plasmon-induced electron transfer from gold nanodots into TiO_2 nanoparticles, *J. Am. Chem. Soc.*, 2007, **129**, 14852-14853.
48. A. Giugni, B. Torre, A. Toma, M. Francardi, M. Malerba, A. Alabastri, R. P. Zaccaria, M. I. Stockman and E. D. Fabrizio, Hot-electron nanoscopy using adiabatic compression of surface plasmons, *Nat. Nanotechnol.*, 2013, **8**, 845-852.
49. Z. Zhu, J. Ma, Z. Wang, C. Mu, Z. Fan, L. Du, Y. Bai, L. Fan, H. Yan and D. L. Phillips, Efficiency enhancement of perovskite solar cells through fast electron

View Article Online
DOI: 10.1039/C6NR09972F

extraction: the role of graphene quantum dots, J. Am. Chem. Soc., 2014, 136, 3760–3763.

50. J.M. Ball, S.D. Stranks, M.T. Hörantner, S. Hüttner, W. Zhang, E.J.W. Crossland, I. Ramirez, M. Riede, M.B. Johnston and R.H. Friend, Optical properties and limiting photocurrent of thin-film perovskite solar cells, *Energ. Environ. Sci.*, 2015, **8**, 602-609.

51. Ghosh and Gorachand., Electronic handbook of optical constants of solids, Academic Press, 1999.

52. W. Fan, B. Yan, Z. Wang and L. Wu, Three-dimensional all-dielectric metamaterial solid immersion lens for subwavelength imaging at visible frequencies, *Sci. Adv*., 2016, **2**, e1600901.

53. Q. Luo, Y. Chen, Z. Li, F. Zhu, X. Chen, Z. Sun, Y. Wei, H. Guo, Z. B. Wang and S. M. Huang, Large enhancements of $NaYF_4$:Yb/Er/Gd nanorod upconversion emissions via coupling with localized surface plasmon of Au film, *Nanotechnology*, 2014, **25**, 185401.

54. M. Bashevoy, V. Fedotov and N. Zheludev, Optical whirlpool on an absorbing metallic nanoparticle, *Opt. Express*, 2005, **13**, 8372-8379.

55. S. K. Cushing, J. Li, F. Meng, T. R. Senty, S.Suri, M. Zhi, M. Li, A. D. Brristow and N. Q. Wu, Photocatalytic activity enhanced by plasmonic resonant energy transfer from metal to semiconductor, *J. Am. Chem. Soc*., 2012, **134**, 15033–15041.

56. J. Li, S. K. Cushing, P. Zheng, F. Meng, D. Chu and N. Wu, Plasmon-induced photonic and energy transfer enhancement of solar water splitting by a hematite nanorod array. *Nature Commun*., 2013, **4**, 2651.

57. L. M. Pazos-Outón, M. Szumilo, R. Lamboll, J. M. Richter, M. Crespo-Quesada, M. Abdi-Jalebi, H. J. Beeson, M. Vrućinić, M. Alsari and H. J. Snaith, Photon recycling in lead iodide perovskite solar cells, *Science*, 2016, **351**, 1430-1433.

58. J. Even, L. Pedesseau and C. Katan, Analysis of Multivalley and Multibandgap Absorption and Enhancement of Free Carriers Related to Exciton Screening in Hybrid Perovskites, *J. Phys. Chem. C,* 2014, **118**, 11566-11572.

View Article Online
DOI: 10.1039/C6NR09972F

59. Q. Lin, A. Armin, R. C. R. Nagiri, P. L. Burn and P. Meredith, Electro-optics of perovskite solar cells, *Nat. Photonics*, 2015, **9**, 106-112.

60. E. Yablonovitch, Lead halides join the top optoelectronic league, *Science*, 2016, **351**, 1401-1401.

61. T. Leijtens, G. E. Eperon, S. Pathak, A. Abate, M. M. Lee and H. J. Snaith, Overcoming Ultraviolet Light Instability of Sensitized TiO_2 with Meso-superstructured Organometal Tri-halide perovskite solar cells, *Nat. Commun*. 2014, **4**, 2885.

62. W. Li, W. Zhang, S. Van Reenen, R. J. Sutton, J. Fan, A. A. Haghighirad, M. B. Johnston, L. Wang and H. J. Snaith, Enhanced UV-light Stability of Planar Heterojunction Perovskite Solar Cells with Caesium Bromide Interface Modification, *Energy Environ. Sci.*, 2016, **9**, 490–498.

63. S. Ito, S. Tanaka, K. Manabe and H. Nishino, Effects of Surface Blocking Layer of Sb_2S_3 on Nanocrystalline TiO_2 for $CH_3NH_3PbI_3$ Perovskite Solar Cells, *J. Phys. Chem. C*, 2014, **118**, 16995-17000.

View Article Online
DOI: 10.1039/C6NR09972F

Figure captions

Fig. 1 (a) *J-V* curves of devices based on p-TiO_2 without and with Au NP and MgO coating. (b) FESEM image of the top surface morphology and (c) cross-sectional FESEM picture of the p-TiO_2 containing Au NPs. (d) Absorbance spectrum of Au suspension. (e) Energy diagram of materials for PSC devices with Au NP and MgO modification.

Fig. 2 (a) UV/Vis absorption and (b) PL spectra of perovskite absorbers based on p-TiO_2 without and with Au NP and MgO coating.

Fig. 3 Dark J-V curves of devices based on p-TiO_2 without and with Au NP and MgO coating.

Fig. 4 (a) Nyquist plots of devices based on p-TiO_2 without and with Au NP and MgO coating under dark condition at 0.9 V applied bias. (b) Simplified equivalent circuit to fit the impedance spectra.

Fig.5 (a) EQE spectra and (b) normalized EQE curves of devices based on p-TiO_2 without and with Au NP and MgO coating. (c) Calculated absorption depth of the absorber as a function of wavelength.

Fig.6 (a) Model of PSC device modified with both Au NPs and MgO. 2D field |E| enhancement distribution image in the *xz* planes at (b) y = 0 nm, λ=560 nm, (c) y= 0 nm, λ=730 nm. Power flow diagrams within the *xz* planes at (d) y = 0 nm, λ=560 nm, (e) y = 10 nm, λ =560 nm, (f) y= 0 nm, λ=730 nm, (g) y=10 nm, λ=730 nm. Power flow diagrams within the *xy* planes at (h) z= 0 nm, λ=730 nm, (g) z=18 nm, λ=730 nm.

View Article Online
DOI: 10.1039/C6NR09972F

Fig. 7 Power conversion efficiency variation of unsealed PSCs based on mesoporous TiO_2 with and without Au NPs and MgO modification at ~55% humidity after various UV exposure durations (90 $mWcm^{-2}$ at 365 nm) durations.

Table 1 Parameters of PSCs based on mesoporous TiO_2 with and without Au NP and MgO modification.

Table 2 EIS results of PSCs based on mesoporous TiO_2 with and without Au NPs and MgO modification.